Measurement of prominent eta-decay branching fractions

A. Lopez, S. Mehrabyan, H. Mendez, J. Ramirez, J. Y. Ge, D. H. Miller, B. Sanghi, I. P. J. Shipsey, B. Xin, G. S. Adams, M. Anderson, J. P. Cummings, I. Danko, D. Hu, B. Moziak, J. Napolitano, Q. He, J. Insler, H. Muramatsu, C. S. Park, E. H. Thorndike, F. Yang, M. Artuso, S. Blusk, S. Khalil, J. Li, N. Menaa, R. Mountain, S. Nisar, K. Randrianarivony, R. Sia, T. Skwarnicki, S. Stone, J. C. Wang, G. Bonvicini, D. Cinabro, M. Dubrovin, A. Lincoln, D. M. Asner, K. W. Edwards, P. Naik, R. A. Briere, T. Ferguson, G. Tatishvili, H. Vogel, M. E. Watkins, J. L. Rosner, N. E. Adam, J. P. Alexander, D. G. Cassel, J. E. Duboscq, R. Ehrlich, L. Fields, R. S. Galik, L. Gibbons, R. Gray, S. W. Gray, D. L. Hartill, B. K. Heltsley, D. Hertz, C. D. Jones, J. Kandaswamy, D. L. Kreinick, V. E. Kuznetsov, H. Mahlke-Kruer, D. Mohapatra, P. U. E. Onyisi, J. R. Patterson, D. Peterson, D. Riley, A. Ryd, A. J. Sadoff, X. Shi, S. Stroiney, W. M. Sun, T. Wilksen, S. B. Athar, R. Patel, J. Yelton, P. Rubin, B. I. Eisenstein, I. Karliner, N. Lowrey, M. Selen, E. J. White, J. Wiss, R. E. Mitchell, M. R. Shepherd, D. Besson, T. K. Pedlar, D. Cronin-Hennessy, K. Y. Gao, J. Hietala, Y. Kubota, T. Klein, B. W. Lang, R. Poling, A. W. Scott, P. Zweber, S. Dobbs, Z. Metreveli, K. K. Seth, A. Tomaradze, J. Ernst, K. M. Ecklund, H. Severini, W. Love, and V. Savinov

Measurement of Prominent η-Decay Branching Fractions

A. Lopez,[1] S. Mehrabyan,[1] H. Mendez,[1] J. Ramirez,[1] J. Y. Ge,[2] D. H. Miller,[2] B. Sanghi,[2] I. P. J. Shipsey,[2] B. Xin,[2]
G. S. Adams,[3] M. Anderson,[3] J. P. Cummings,[3] I. Danko,[3] D. Hu,[3] B. Moziak,[3] J. Napolitano,[3] Q. He,[4] J. Insler,[4]
H. Muramatsu,[4] C. S. Park,[4] E. H. Thorndike,[4] F. Yang,[4] M. Artuso,[5] S. Blusk,[5] S. Khalil,[5] J. Li,[5] N. Menaa,[5] R. Mountain,[5]
S. Nisar,[5] K. Randrianarivony,[5] R. Sia,[5] T. Skwarnicki,[5] S. Stone,[5] J. C. Wang,[5] G. Bonvicini,[6] D. Cinabro,[6] M. Dubrovin,[6]
A. Lincoln,[6] D. M. Asner,[7] K. W. Edwards,[7] P. Naik,[7] R. A. Briere,[8] T. Ferguson,[8] G. Tatishvili,[8] H. Vogel,[8] M. E. Watkins,[8]
J. L. Rosner,[9] N. E. Adam,[10] J. P. Alexander,[10] D. G. Cassel,[10] J. E. Duboscq,[10] R. Ehrlich,[10] L. Fields,[10] R. S. Galik,[10]
L. Gibbons,[10] R. Gray,[10] S. W. Gray,[10] D. L. Hartill,[10] B. K. Heltsley,[10] D. Hertz,[10] C. D. Jones,[10] J. Kandaswamy,[10]
D. L. Kreinick,[10] V. E. Kuznetsov,[10] H. Mahlke-Krüger,[10] D. Mohapatra,[10] P. U. E. Onyisi,[10] J. R. Patterson,[10]
D. Peterson,[10] D. Riley,[10] A. Ryd,[10] A. J. Sadoff,[10] X. Shi,[10] S. Stroiney,[10] W. M. Sun,[10] T. Wilksen,[10] S. B. Athar,[11]
R. Patel,[11] J. Yelton,[11] P. Rubin,[12] B. I. Eisenstein,[13] I. Karliner,[13] N. Lowrey,[13] M. Selen,[13] E. J. White,[13] J. Wiss,[13]
R. E. Mitchell,[14] M. R. Shepherd,[14] D. Besson,[15] T. K. Pedlar,[16] D. Cronin-Hennessy,[17] K. Y. Gao,[17] J. Hietala,[17]
Y. Kubota,[17] T. Klein,[17] B. W. Lang,[17] R. Poling,[17] A. W. Scott,[17] P. Zweber,[17] S. Dobbs,[18] Z. Metreveli,[18] K. K. Seth,[18]
A. Tomaradze,[18] J. Ernst,[19] K. M. Ecklund,[20] H. Severini,[21] W. Love,[22] and V. Savinov[22]

(CLEO Collaboration)

[1]*University of Puerto Rico, Mayaguez, Puerto Rico 00681*
[2]*Purdue University, West Lafayette, Indiana 47907, USA*
[3]*Rensselaer Polytechnic Institute, Troy, New York 12180, USA*
[4]*University of Rochester, Rochester, New York 14627, USA*
[5]*Syracuse University, Syracuse, New York 13244, USA*
[6]*Wayne State University, Detroit, Michigan 48202, USA*
[7]*Carleton University, Ottawa, Ontario, Canada K1S 5B6*
[8]*Carnegie Mellon University, Pittsburgh, Pennsylvania 15213, USA*
[9]*Enrico Fermi Institute, University of Chicago, Chicago, Illinois 60637, USA*
[10]*Cornell University, Ithaca, New York 14853, USA*
[11]*University of Florida, Gainesville, Florida 32611, USA*
[12]*George Mason University, Fairfax, Virginia 22030, USA*
[13]*University of Illinois, Urbana-Champaign, Illinois 61801, USA*
[14]*Indiana University, Bloomington, Indiana 47405, USA*
[15]*University of Kansas, Lawrence, Kansas 66045, USA*
[16]*Luther College, Decorah, Iowa 52101, USA*
[17]*University of Minnesota, Minneapolis, Minnesota 55455, USA*
[18]*Northwestern University, Evanston, Illinois 60208, USA*
[19]*State University of New York at Albany, Albany, New York 12222, USA*
[20]*State University of New York at Buffalo, Buffalo, New York 14260, USA*
[21]*University of Oklahoma, Norman, Oklahoma 73019, USA*
[22]*University of Pittsburgh, Pittsburgh, Pennsylvania 15260, USA*

The decay $\psi(2S) \rightarrow \eta J/\psi$ is used to measure, for the first time, all prominent η-meson branching fractions with the same experiment in the same dataset, thereby providing a consistent treatment of systematics across branching fractions. We present results for η decays to $\gamma\gamma$, $\pi^+\pi^-\pi^0$, $3\pi^0$, $\pi^+\pi^-\gamma$ and $e^+e^-\gamma$, accounting for 99.9% of all η decays. The precision of several of the branching fractions and their ratios is improved. Two channels, $\pi^+\pi^-\gamma$ and $e^+e^-\gamma$, show results that differ at the level of three standard deviations from those previously determined.

The η meson was discovered almost half a century ago [1]. It is the second-lightest meson, considered to consist of u, d, and s quarks, and studying its decays into pions, electrons, and photons gives insight into different aspects of nonperturbative QCD and electromagnetic phenomena.

Measurements of the η decay properties come from many different experiments, and almost all exclusive branching fraction determinations are made relative to other η decays. The Particle Data Group (PDG) [2] uses 43 such measurements in a fit to determine the branching fractions
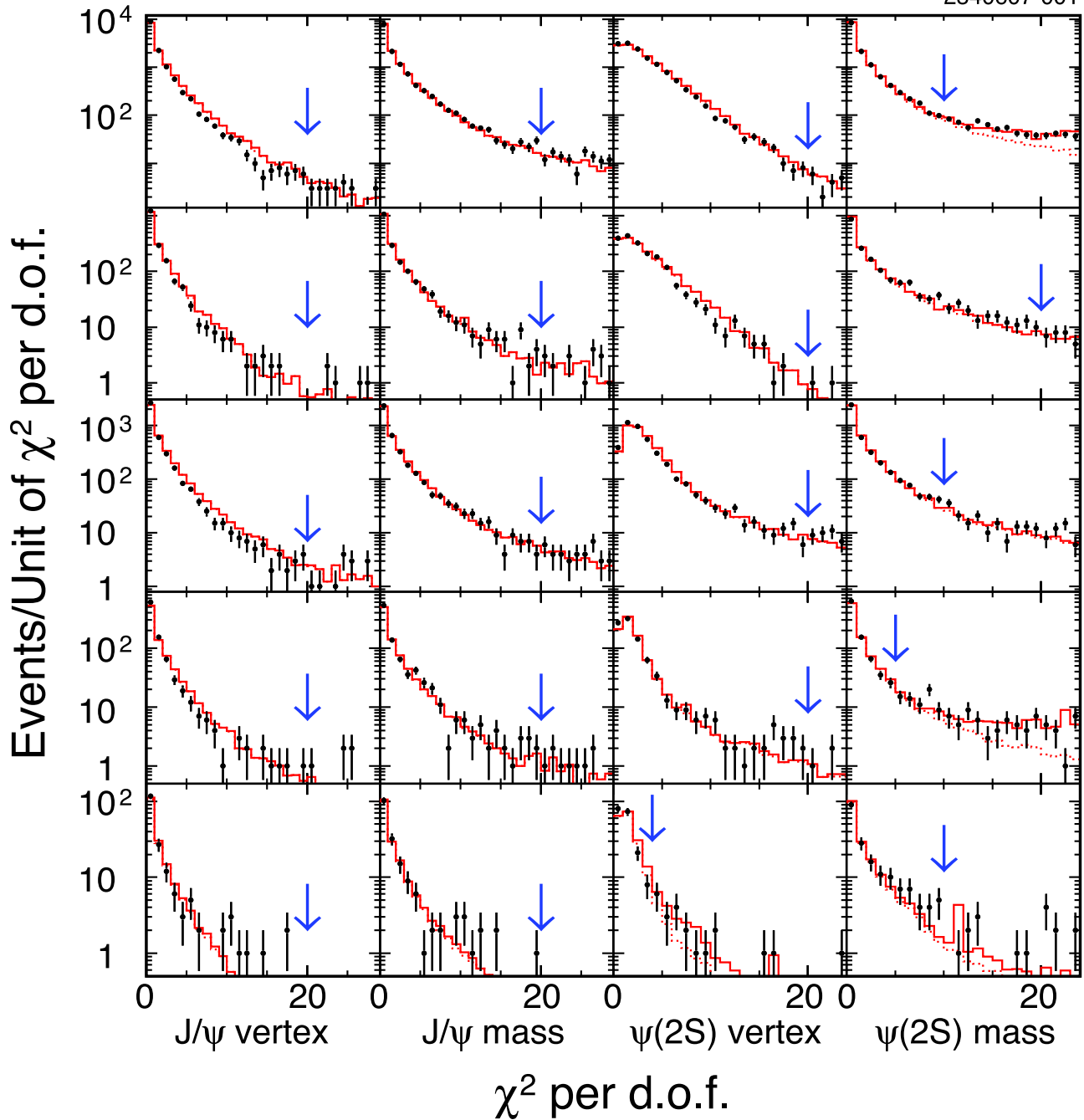
2540607-001

FIG. 1 (color online).   Top to bottom: $\gamma\gamma$, $3\pi^0$, $\pi^+\pi^-\pi^0$, $\pi^+\pi^-\gamma$, $e^+e^-\gamma$. For each channel, left to right: Goodness-of-fit for J/ψ vertex and mass fit, and for $\psi(2S)$ vertex and mass fit. Points: data. Dotted line: Signal MC predictions. Solid line: Sum of all MC predictions. Arrows indicate selection requirements. Cuts have been applied to all quantities with the exception of the one plotted.

to $\gamma\gamma$, $3\pi^0$, $\pi^+\pi^-\pi^0$, $\pi^+\pi^-\gamma$, $\pi^0\gamma\gamma$, $e^+e^-\gamma$, $\mu^+\mu^-\gamma$, and $\pi^+\pi^-e^+e^-$, as well as the total width.

The analysis presented here studies η decays in the reaction $e^+e^- \rightarrow \psi(2S) \rightarrow \eta J/\psi$ with $\eta \rightarrow \gamma\gamma$, $3\pi^0$, $\pi^+\pi^-\pi^0$, $\pi^+\pi^-\gamma$, and $e^+e^-\gamma$. We identify the J/ψ through its decays to e^+e^- and $\mu^+\mu^-$. The choice of modes addresses the known branching fractions of $\mathcal{O}(0.1\%)$ and larger, and covers 99.88% of the η decay

modes when using the branching fractions from Ref. [2]. The strength of this analysis lies in the simultaneous and similar treatment of charged and neutral η decay products, cross-feed of different modes into each other, and, with the same analysis procedure, estimates of backgrounds from other XJ/ψ sources.

The CLEO-c detector is described in detail elsewhere [3]. Its features exploited here are the 93% solid angle

coverage of precision charged particle tracking and an electromagnetic calorimeter consisting of 7784 CsI(Tl) crystals, the barrel portion of which has a vertex-pointing geometry. The barrel calorimeter and two open-cell drift chambers are concentric with the colliding beams and embedded inside a 1 T axial magnetic field provided by a superconducting solenoid. The small inner chamber has six cylindrical stereo layers (drift cells canted at an angle to the chamber axis), and the outer, larger chamber has 47 layers, the inner 16 of which are axial and the outer 31 stereo. (About 5% of the data used here were acquired in the earlier CLEO III detector configuration, which differed from CLEO-c primarily by having a four-layer silicon strip vertex detector in place of the inner tracking chamber.) The tracking system enables momentum measurements for particles with momentum transverse to the beam exceeding 50 MeV/c and achieves resolution $\sigma_p/p \simeq 0.6\%$ at $p = 1$ GeV/c. The barrel calorimeter reliably measures photon shower energies down to $E_\gamma = 30$ MeV and has a resolution of $\sigma_E/E \simeq 5\%$ at 100 MeV and 2.2% at 1 GeV.

The data sample comprises about 27 M $\psi(2S)$ decays, corresponding to about 0.1 M η decays produced with a $J/\psi \to \ell^+\ell^-$ tag.

We determine the detection efficiency and background levels with Monte Carlo (MC) samples that were generated using the EVTGEN event generator [4] and a GEANT-based [5] detector simulation. We model $\eta \to \gamma\gamma$ and $3\pi^0$ according to phase space. The mode $\pi^+\pi^-\gamma$ is simulated as mediated by a $\rho^0 \to \pi^+\pi^-$ decay, weighted with a factor $\sim E_\gamma^3$, where E_γ is the photon energy in the η center-of-mass system. We generate $\pi^+\pi^-\pi^0$ according to the distribution measured in [6]. The simulation of $e^+e^-\gamma$ is analogous to $\pi^0 \to e^+e^-\gamma$ ("Dalitz decay") [7].

The event selection proceeds as follows. We select the $J/\psi \to \ell^+\ell^-$ track candidates within polar angles $|\cos\theta_{\ell^\pm}| < 0.83$, adding bremsstrahlung photons within a cone of 100 mrad around the track momentum vector at the collision point. We identify leptons through the ratio of energy deposition in the calorimeter associated with the track, E, to the track momentum measured in the drift chamber, p: For electron (muon) candidates, we require E/p values of >0.85 (<0.25) for one lepton and >0.50 (<0.50) for the other. We impose kinematic constraints by fitting the two lepton candidates to a common originating vertex (where the figure of merit is given by $\chi^2_{J/\psi,v}$/d.o.f.) and to the J/ψ mass ($\chi^2_{J/\psi,m}$/d.o.f.). We keep candidates that have $\chi^2_{J/\psi,v}$/d.o.f. < 20 and $\chi^2_{J/\psi,m}$/d.o.f. < 20, which keeps signal decays with high efficiency, as evident from Fig. 1. The photons in the η decay products are required to be in the region of best calorimeter performance and least material in front of the crystals, $|\cos\theta_\gamma| < 0.75$, and not be matched or close to a track's projection into the calorimeter.

We then proceed to use kinematic constraints once more for improved event cleanliness: The fitted J/ψ and the η decay products are constrained, together with the beam spot [8], to a common vertex, and then to the $\psi(2S)$ mass. This results in a very clean separation of final states. We apply mode-dependent restrictions on the quality of these fits, denoted by $\chi^2_{\psi(2S),v}$/d.o.f. and $\chi^2_{\psi(2S),m}$/d.o.f., respectively. Conversion events originating from $\eta \to \gamma\gamma$ decay can fulfil the $e^+e^-\gamma$ preselection, but have a poor $\psi(2S)$ vertex fit; hence, we apply a stricter cut of $\chi^2_{\psi(2S),v}$/d.o.f. < 4 in this channel (see Fig. 1). All other modes require $\chi^2_{\psi(2S),v}$/d.o.f. < 20. The mass fit has mode-dependent cuts, set as loosely as possible while preserving sample cleanliness: $\chi^2_{\psi(2S),m}$/d.o.f. < 20 for $\pi^+\pi^-\pi^0$, <10 for $\gamma\gamma$, $3\pi^0$, and $e^+e^-\gamma$, <5 for $\pi^+\pi^-\gamma$.

After this step, we define the following signal windows: $p(J/\psi) = 170$–230 MeV/c, and two ranges for $m(\eta)$: 542–554 MeV for $\pi^+\pi^-\gamma$, 535–560 MeV for all others. Final state specific characteristics are (1) $\gamma\gamma$: $E_\gamma > 200$ MeV, to suppress photons from $\psi(2S) \to \gamma\chi_{c1}$. (2) $\pi^+\pi^-\pi^0$: We search for two photons with $E_\gamma > 30$ MeV and $m(\gamma\gamma) = 100$–160 MeV, and constrain
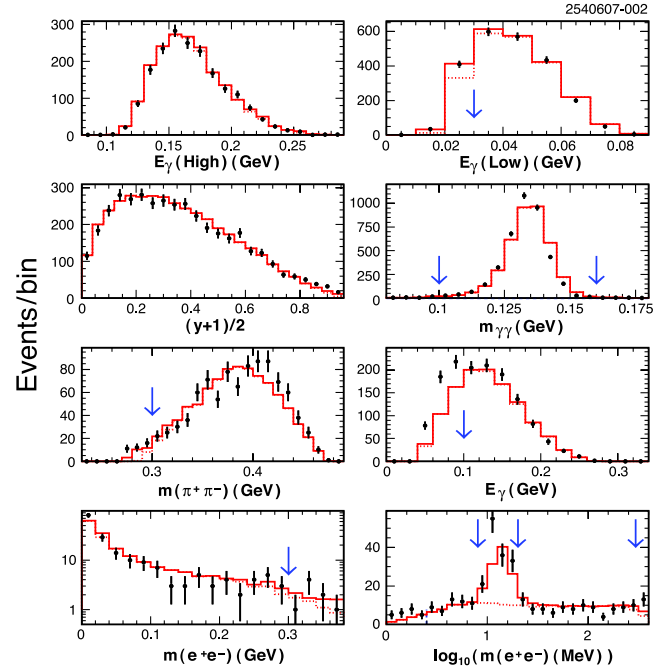

FIG. 2 (color online). Distributions for individual channels. Top row: $3\pi^0$, highest and lowest photon energies. Second row: $\pi^+\pi^-\pi^0$, kinematic distribution of the three pions, and two-photon invariant mass; y is a function of the kinetic energy of the π^0 (T_0) and the sum of the kinetic energies of all pions (Q): $y = (3T_0/Q) - 1$. Third row: $\pi^+\pi^-\gamma$, invariant mass of the two pions and photon energy. Fourth row: $e^+e^-\gamma$, invariant mass of the two electrons on different horizontal and vertical scales. Symbols as in Fig. 1.
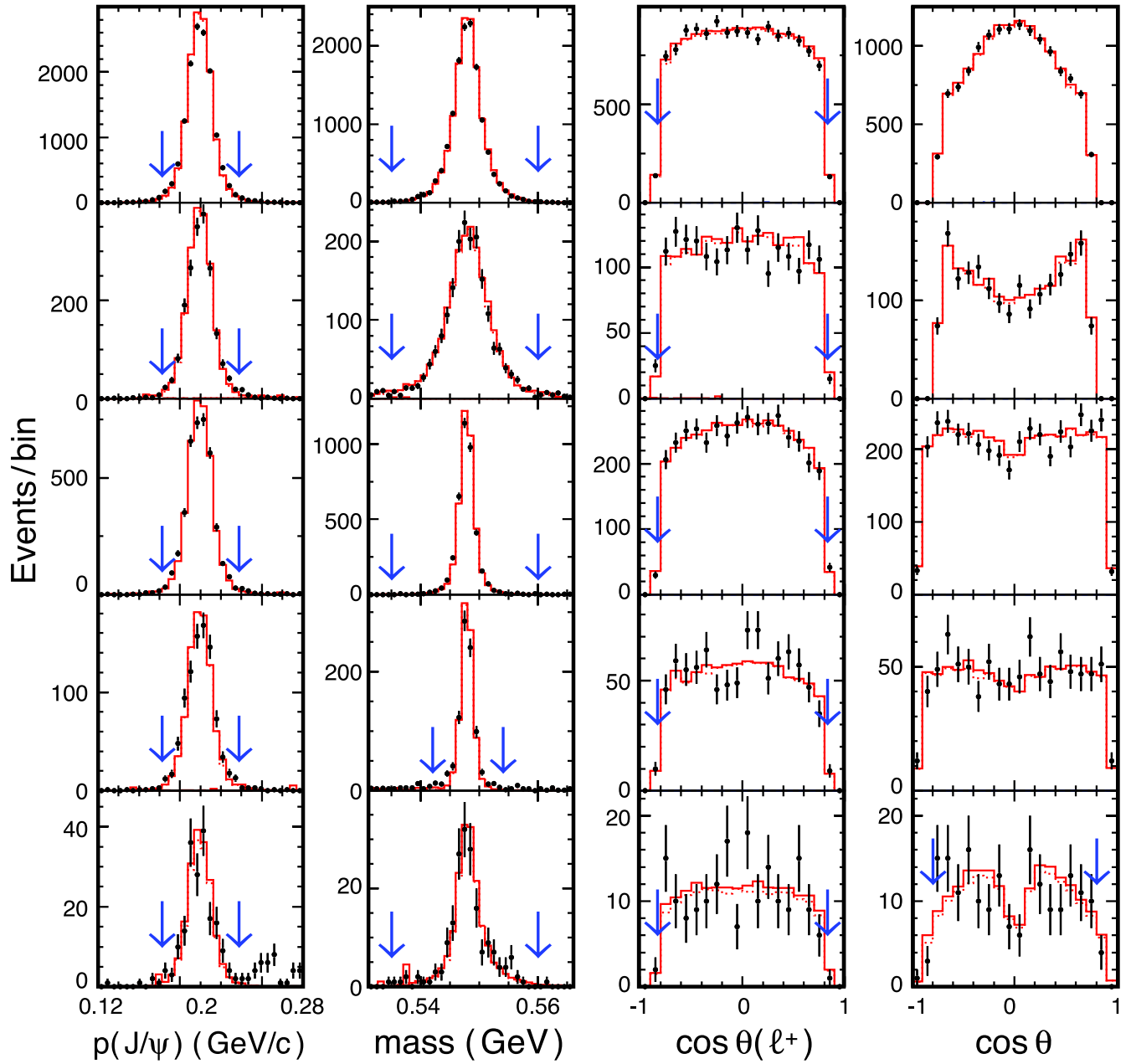
2540607-003

FIG. 3 (color online).   Top to bottom: $\gamma\gamma$, $3\pi^0$, $\pi^+\pi^-\pi^0$, $\pi^+\pi^-\gamma$, $e^+e^-\gamma$. For each channel, left to right: J/ψ momentum, η mass, polar angle of the positive lepton from the J/ψ decay, and polar angle of an η decay product (most energetic shower for $\gamma\gamma$ and $3\pi^0$, positive track for $\pi^+\pi^-\pi^0$, $\pi^+\pi^-\gamma$, and $e^+e^-\gamma$). Symbols as in Fig. 1.

them to the π^0 mass. (3) $3\pi^0$: We search for six photons, but do not attempt to make assignments to π^0 candidates because doing so typically results in multiple comparably probable assignments. (4) $\pi^+\pi^-\gamma$: $E_\gamma > 100$ MeV and $m(\pi^+\pi^-) > 300$ MeV. (5) $e^+e^-\gamma$: We add bremsstrahlung photons to the soft electrons as with $J/\psi \to \ell^+\ell^-$, and the soft $e^\pm$ tracks must satisfy $|\cos\theta| < 0.8$. In addition, we require $m(e^+e^-) < 300$ MeV. A substantial number of $\gamma\gamma$ events with a conversion survive the vertex restriction described above and fake the $e^+e^-\gamma$ signature;

indeed, this type of background has necessitated substantial subtractions in previous measurements of this mode [9,10]. These conversions tend to occur at the discrete locations such as the beam pipe and tracking chamber boundaries, but are reconstructed as if they originated at the interaction point. Consequently, they create an artificial mass peak near 10 MeV as seen in the lower right of Fig. 2. We remove the mass region $m(e^+e^-) = 8$–20 MeV to suppress this background and the systematic uncertainties associated with it.

For all five η decay channels, we keep the two J/ψ decay modes separate. The fit quality for data and simulation is compared in Fig. 1. As a cross-check, we also perform the analysis *without* the $\psi(2S)$ kinematic fit: consistent results are obtained, but in most modes with far worse background conditions and larger uncertainties.

The main backgrounds arise from cross-feed between the η modes and from other $\psi(2S) \to XJ/\psi$ transitions, mostly $X = \pi^+\pi^-$, $\pi^0\pi^0$, and $\gamma\gamma$ through χ_{cJ}. We select such exclusive event samples using selections similar to the η signal decays, including the kinematic fits. Backgrounds from these XJ/ψ channels into the η signals are then determined by scaling the MC predictions so as to match the observed XJ/ψ yields in data, and subtracted. The statistical uncertainties of these subtractions are accounted for. We find that $\gamma\gamma$, $3\pi^0$, $\pi^+\pi^-\pi^0$, and $\pi^+\pi^-\gamma$ have such backgrounds at the levels of 1–2%. Examination of the η mass sidebands revealed no discrepancy between data yields and MC estimate; the only exception is $\pi^+\pi^-\gamma$, where data exceed MC estimates by an amount which, when extrapolated into the signal region, corresponds to a background of $(2.8 \pm 1.1)\%$ and is subtracted in addition to the predictions from the Monte Carlo simulation. The mode $e^+e^-\gamma$ has a background of about 5% due mostly to $\gamma\gamma$ conversions which survived the $m(e^+e^-)$ and tight vertex fit restrictions. Other (non-J/ψ) $\psi(2S)$ decays do not fake the signal signature at any appreciable level. We use a 20.7 pb^{-1} sample of data taken at a center-of-mass energy of 3.670 GeV to estimate continuum background (scaled by luminosity and energy dependence), which is found to be negligible.

All inspected experimental observables show good agreement between data and the sum of our MC samples, normalized according to their relative population in the data. A selection of comparisons is shown in Figs. 2 and 3.

Table I lists observed yields and the estimated background. We observe significant, clean, and unambiguous signals for all our target modes.

Our measurements are performed as ratios between efficiency-corrected event yields of pairs of η final states, separately for $J/\psi \to e^+e^-$ and $\mu^+\mu^-$. This allows cancellation of all lepton-related systematic uncertainties, such as track finding, lepton identification, and J/ψ fitting. We then proceed to combine the two measurements of each ratio, where the η-related uncertainties are treated as fully correlated. We note that the absolute detection efficiency for $\psi(2S) \to \eta J/\psi$, $\eta \to \gamma\gamma$, $J/\psi \to \ell^+\ell^-$ is about one-third.

Sources of systematic uncertainty and the values assigned are: Track finding (0.3% per track, added linearly [11]), photon finding (0.4% per photon, added linearly [11]), sideband subtraction (1.1%, $\pi^+\pi^-\gamma$ only), trigger (0.1–0.5%, mode-dependent), and MC statistics (0.4–1.0%, mode-dependent), other effects in the detector simulation (0.5%). We also make reasonable variations in decay

TABLE I. For each η decay channel, the observed yields in the $\psi(2S)$ on-resonance sample ($N^{\psi(2S)}$), background from cross-feed between η modes (N^{cf}), and background from other XJ/ψ decays ($N^{XJ/\psi}$) separately for $J/\psi \to ee$ and $J/\psi \to \mu\mu$.

Channel	$N^{\psi(2S)} - N^{\mathrm{cf}} - N^{XJ/\psi}$	
	$J/\psi \to e^+e^-$	$J/\psi \to \mu^+\mu^-$
$\gamma\gamma$	$6324 - 0 - 66$	$7376 - 0 - 114$
$3\pi^0$	$850 - 0 - 18$	$1004 - 0 - 15$
$\pi^+\pi^-\pi^0$	$1884 - 4 - 12$	$2052 - 5 - 0$
$\pi^+\pi^-\gamma$	$403 - 3 - 17$	$498 - 2 - 20$
$e^+e^-\gamma$	$82 - 4 - 0$	$100 - 6 - 0$

modeling at the MC generator level and assign uncertainties accordingly: 0.1% for $3\pi^0$ to account for the slight deviation from phase-space-prescribed decay observed in Ref. [12], 0.9% for $\pi^+\pi^-\pi^0$ based on the experimental uncertainty of the slope parameter in Ref. [6], 3% for $\pi^+\pi^-\gamma$ to include a slightly different line shape parameterization of the intermediate ρ^0 meson, and 5% for $e^+e^-\gamma$ to allow for changes in the polar angle distribution of the e^+ from the η decay and in the $m(e^+e^-)$ spectrum that remain consistent with our measurements. All uncertainties are added in quadrature, except where correlations between modes have been observed.

The results for ratios of branching fractions are shown in Table II. The χ^2 for the ratios relative to $\gamma\gamma$ to agree between $J/\psi \to e^+e^-$ and $\mu^+\mu^-$ is 5.9 for 4 degrees of freedom, corresponding to a confidence level of ~20%. We designate the following four ratios as constituting a complete set, having minimal systematic correlation with each other: $3\pi^0/\gamma\gamma$, $\pi^+\pi^-\pi^0/\gamma\gamma$, $\pi^+\pi^-\gamma/\pi^+\pi^-\pi^0$, and $e^+e^-\gamma/\pi^+\pi^-\gamma$. We compare to the single most precise other measurements in Fig. 4.

Under the assumption that our five signal modes account for all of the η decay modes, we combine the ratios

TABLE II. Ratios of η branching fractions. For each combination, the efficiency ratio, separately for $J/\psi \to e^+e^-$ and $J/\psi \to \mu^+\mu^-$, the level of consistency between the $J/\psi \to e^+e^-$ and $\mu^+\mu^-$ result, expressed in units of Gaussian standard deviations, $\sigma_{\mu\mu/ee}$, and the combined result for the branching ratio. The dagger symbol indicates that this result is the most precise measurement to date.

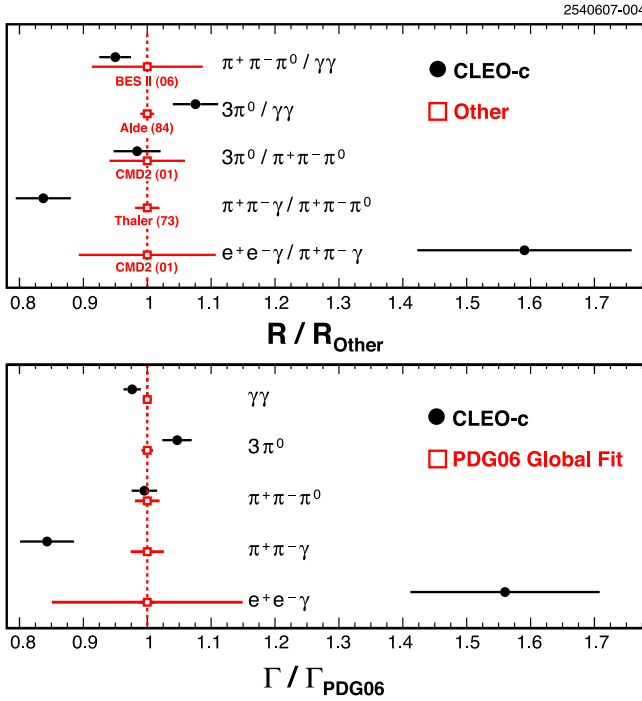| Channel	eff. ratio		$\sigma_{\mu\mu/ee}$	branching fraction ratio
	$\mu\mu$	ee		
$3\pi^0/\gamma\gamma$	0.15	0.15	1.0	$0.884 \pm 0.022 \pm 0.019$
$\pi^+\pi^-\pi^0/\gamma\gamma$	0.50	0.49	-2.2	$0.587 \pm 0.011 \pm 0.009^{\dagger}$
$\pi^+\pi^-\gamma/\gamma\gamma$	0.63	0.60	0.2	$0.103 \pm 0.004 \pm 0.004^{\dagger}$
$e^+e^-\gamma/\gamma\gamma$	0.53	0.52	0.1	$0.024 \pm 0.002 \pm 0.001^{\dagger}$
$3\pi^0/\pi^+\pi^-\pi^0$	0.30	0.32	2.1	$1.496 \pm 0.043 \pm 0.035^{\dagger}$
$\pi^+\pi^-\gamma/\pi^+\pi^-\pi^0$	1.27	1.24	1.1	$0.175 \pm 0.007 \pm 0.006$
$e^+e^-\gamma/\pi^+\pi^-\pi^0$	1.07	1.06	0.5	$0.041 \pm 0.003 \pm 0.002^{\dagger}$
$e^+e^-\gamma/\pi^+\pi^-\gamma$	0.84	0.86	0.0	$0.237 \pm 0.021 \pm 0.015$

FIG. 4 (color online). Comparison of the results obtained in this analysis with the most precise measurements from other experiments [2,14] (top) and the PDG 2006 global fits [2].

between them to form absolute branching fraction measurements. Correlations between uncertainties are taken into account. Other possible η decay modes are either forbidden and/or have been found to be below 0.2% in branching fraction [2]: We include 0.3% as a systematic uncertainty in the absolute branching fraction results. The results are presented in Table III, together with those from PDG 2006 [2] for the global fit to all measurements. In all five modes, the statistical uncertainty is larger than or comparable to the systematic error. A visual comparison can be found in Fig. 4.

To summarize, we have studied five η decay modes using the decay chain $\psi(2S) \rightarrow \eta J/\psi$, $J/\psi \rightarrow ee$, and $\mu\mu$: $\eta \rightarrow \gamma\gamma$, $3\pi^0$, $\pi^+\pi^-\pi^0$, $\pi^+\pi^-\gamma$, and $e^+e^-\gamma$. We have presented ratios between these modes as well as

TABLE III. For each η decay channel, absolute branching fraction measurements for $J/\psi \rightarrow e^+e^-$ and $J/\psi \rightarrow \mu^+\mu^-$ combined, with statistical and systematic uncertainties (middle column), as determined in this Letter. The last column shows the PDG fit result [2]. All but $\gamma\gamma$ are first measurements [13].

Channel	this work (%)	PDG [2] (%)
$\gamma\gamma$	$38.45 \pm 0.40 \pm 0.36$	39.38 ± 0.26
$3\pi^0$	$34.03 \pm 0.56 \pm 0.49$	32.51 ± 0.28
$\pi^+\pi^-\pi^0$	$22.60 \pm 0.35 \pm 0.29$	22.7 ± 0.4
$\pi^+\pi^-\gamma$	$3.96 \pm 0.14 \pm 0.14$	4.69 ± 0.11
$e^+e^-\gamma$	$0.94 \pm 0.07 \pm 0.05$	0.60 ± 0.08

absolute η branching fractions to these final states. This is the first analysis that covers this range of η decay modes, summing up to 99.9% of the known η decays, and determines their absolute branching fractions in the same experiment. Several of the relative and derived absolute branching fractions obtained in this analysis are either the most precise to date or first measurements. In particular, we note that our result for $\pi^+\pi^-\gamma$ is about $\sim$15% (3.2σ) smaller than previous measurements, and for $e^+e^-\gamma$ is $\sim$57% (2.9σ) larger.

[1] A. Pevsner *et al.*, Phys. Rev. Lett. **7**, 421 (1961).
[2] W. M. Yao *et al.* (Particle Data Group), J. Phys. G **33**, 1 (2006).
[3] R. A. Briere *et al.* (CESR-c and CLEO-c Taskforces, CLEO-c Collaboration), Cornell University, LEPP Report No. CLNS 01/1742, 2001 (unpublished); G. Viehhauser, Nucl. Instrum. Methods Phys. Res., Sect. A **462**, 146 (2001); M. Artuso *et al.*, Nucl. Instrum. Methods Phys. Res., Sect. A **554**, 147 (2005); D. Peterson *et al.*, Nucl. Instrum. Methods Phys. Res., Sect. A **478**, 142 (2002).
[4] D. J. Lange, Nucl. Instrum. Methods Phys. Res., Sect. A **462**, 152 (2001).
[5] R. Brun *et al.*, Geant 3.21, CERN Program Library Long Writeup Report No. W5013, 1993 (unpublished).
[6] J. G. Layter *et al.*, Phys. Rev. D **7**, 2565 (1973).
[7] A. Faessler, C. Fuchs, and M. I. Krivoruchenko, Phys. Rev. C **61**, 035206 (2000).
[8] The beam spot is the center of the ellipsoidal e^+e^- collision region, and is determined from finding a common vertex position in hadronic events that occur in contiguous 30–60 min periods of stable beam conditions.
[9] R. R. Akhmetshin *et al.* (CMD-2 Collaboration), Phys. Lett. B **501**, 191 (2001).
[10] M. N. Achasov, V. M. Aulchenko, K. I. Beloborodov, and A. V. Berdyugin, Phys. Lett. B **504**, 275 (2001).
[11] N. E. Adam *et al.* (CLEO Collaboration), Phys. Rev. Lett. **94**, 232002 (2005).
[12] W. B. Tippens *et al.* (Crystal Ball Collaboration), Phys. Rev. Lett. **87**, 192001 (2001).
[13] Although PDG 2006 [2] lists two absolute measurements [9,10] for $\eta \rightarrow e^+e^-\gamma$, both rely on previously measured exclusive η branching fractions and therefore are inherently relative, not absolute, measurements.
[14] M. Ablikim *et al.* (BES Collaboration), Phys. Rev. D **73**, 052008 (2006); D. Alde *et al.*, Z. Phys. C **25**, 225 (1984); Yad. Fiz. **40**, 1447 (1984); R. R. Akhmetshin *et al.* (CMD-2 Collaboration), Phys. Lett. B **509**, 217 (2001); J. J. Thaler *et al.*, Phys. Rev. D **7**, 2569 (1973).